



# Parameterizing the fresh-water flux from land ice to ocean with interactive icebergs in a coupled climate model

T. Martin <sup>\*,1</sup>, A. Adcroft

Princeton University, Atmospheric and Oceanic Sciences Program, 201 Forrestal Road, Princeton, NJ 08540, USA

## ARTICLE INFO

### Article history:

Received 27 January 2010

Received in revised form 16 April 2010

Accepted 10 May 2010

Available online 26 May 2010

### Keywords:

Coupled climate model

Fresh-water flux

Calving

Icebergs

Deep-water formation

Southern Ocean

Antarctica

Greenland

## ABSTRACT

Icebergs are an important part of the fresh-water cycle and, until now, have not been explicitly represented in Intergovernmental Panel on Climate Change (IPCC) class coupled global circulation models (CGCMs) of the climate system. In this study we examine the impact of introducing interactive icebergs in a next-generation CGCM designed for 21st Century climate predictions. The frozen fresh-water discharge from land is used as calving to create icebergs in the coupled system which are then free to evolve and interact with the sea-ice and ocean components. Icebergs are fully prognostic, represented as point particles and evolve according to momentum and mass balance equations. About 100,000 individual particles are present at any time in the simulations but represent many more icebergs through a clustering approach. The various finite sizes of icebergs, which are prescribed by a statistical distribution at the calving points, lead to a finite life-time of icebergs ranging from weeks, for the smallest icebergs (60 m length), up to years for the largest (2.2 km length). The resulting melt water distribution seen by the ocean enhances deep-water formation, in particular on the continental shelves, relative to the model without icebergs.

© 2010 Elsevier Ltd. All rights reserved.

## 1. Introduction

Calving of icebergs at the edge of glaciers and ice shelves is thought to account for as much as 50% of the net fresh-water flux from land ice to the ocean in Greenland, and 60–80% in the Antarctic (Hooke, 2005; Schodlok et al., 2006). The other principle mechanisms are surface melt in Greenland and bottom melt at the interface between the ice shelf and ocean in the Antarctic. Total mass loss from Antarctica and Greenland is estimated at  $3200 \pm 400 \text{ Gt year}^{-1}$  of which  $2300 \pm 300 \text{ Gt year}^{-1}$  is estimated to be due to calving alone (cf. Hooke, 2005, his Table 3.2). Although there is great uncertainty in these estimates, due to the challenge of making such observations, there is no doubt that calving and icebergs represent a significant pathway in the fresh-water cycle of the polar oceans.

In recent years, coupled global circulation models (CGCMs) of the climate system have striven to close the mass and energy budgets as well as possible. Only very few contemporary comprehensive CGCMs do already include an explicit model of ice sheets or ice shelves or a representation of interactive icebergs, but none actually include both. Precipitation over glaciated regions is often treated as excess fresh water (which would actually accumulate into

an ice sheet in the real world) and is arbitrarily transported to the ocean. The choice of what to do with this excess fresh water is also arbitrary and greatly varies between models. An early and still often applied approach to close the fresh-water cycle is to redistribute this fresh-water excess uniformly and instantaneously across the global ocean (e.g. Boville and Gent, 1998). In a more advanced, but rarely used approach in the Hadley Center's Climate Model version 3 (HadCM3) the recirculation of excess precipitation is restricted to high latitude oceans, i.e. north of  $40^\circ\text{N}$  and south of  $50^\circ\text{S}$  (Weber et al., 2007). Although locally uniform in space this redistribution scheme also accounts for regional differences in the fresh-water flux from nearby ice sheets and is based on an estimated mean distribution of icebergs (Gordon et al., 2000).

In contrast, modern CGCMs have river networks, which are implemented in the land model, to transport the excess fresh water and bridge the gap. For example, in one approach all solid (or frozen) and liquid precipitation, which exceeds a buffer of  $1000\text{--}2000 \text{ kg m}^{-2}$  snow water equivalent (or 1–2 m snow thickness) (Oleson et al., 2004; Weber et al., 2007), is exported in one or more separate variables to the ocean using a river transport model. The runoff is deposited in the coastal ocean at the river mouths. This solution is widely used, for instance in the Community Climate System Model version 3 (CCSM3) (Oleson et al., 2004; Hack et al., 2006), the Climate Model version 2 (CM2.x) of the Geophysical Fluid Dynamics Laboratory (GFDL) (Anderson et al., 2004), and many others (Weber et al., 2007).

\* Corresponding author. Tel.: +49 431 600 4056; fax: +49 431 600 4052.

E-mail address: [ToMartin@ifm-geomar.de](mailto:ToMartin@ifm-geomar.de) (T. Martin).

<sup>1</sup> Now at IFM-GEOMAR, Leibniz Institute of Marine Sciences, Duesternbrooker Weg 20, 24105 Kiel, Germany.

Both approaches used in current CGCMs can be justified: since little is known about the amount and distribution of the solid fresh-water flux from land to ocean (or calving flux) the river runoff scheme does not prescribe any unknown quantity but simply closes the fresh-water cycle. However, this approach implicitly assumes that the implied ice sheet is in instantaneous equilibrium. In contrast, the approach taken by [Gordon et al. \(2000\)](#) helps to minimize the bias of incorrect cold-fresh forcing by spreading out the forcing while keeping it spatially restrained to ocean areas that are naturally affected by a calving flux. Regardless of the choice of frozen discharge distribution, no comprehensive coupled model has an explicit representation of interactive icebergs.

In the real world, the calved mass takes the form of icebergs and ultimately enters the ocean in liquid form via the process of iceberg erosion and melt. The two choices for calving distribution described above represent two possible extremes for distributing the cold-fresh water forcing across the ocean. In either case, forcing biases on the ocean should be expected, due to the missing representation of icebergs; in the first instance, spreading out the calving uniformly on the world oceans, the extra-polar regions should have a false, albeit weak, fresh bias and a salty bias where icebergs are supposed to melt. In the latter case of depositing calving into the coastal oceans, a fresh bias might be expected at the coast and a salty bias where the missing icebergs would otherwise melt. In practice, the story is more complicated than this due to a tendency for the frozen discharge deposited into near-freezing Antarctic coastal waters to immediately form sea ice which can then be exported away in frozen form. This might, at first glance, appear to be closer to the way in which icebergs should export frozen water from the Antarctic coast but the finite salinity of sea ice assumed by climate models, ironically, leads to an export of salt relative to the icebergs which leads to a coastal fresh bias.

The distribution of iceberg melt water was estimated by [Bigg et al. \(1997\)](#) for the North Atlantic, and by [Gladstone et al. \(2001\)](#) and [Silva et al. \(2006\)](#) for the Southern Ocean in uncoupled iceberg model experiments. They prescribed a calving flux and simulated the drift and decay of icebergs forced by atmospheric reanalysis data and ocean model output. Recently, [Jongma et al. \(2009\)](#) examined the impact of distributed iceberg melt on the ocean by repeating the experiments of [Bigg et al. \(1997\)](#) and [Gladstone et al. \(2001\)](#) with a coupled atmosphere–sea-ice–ocean model of intermediate complexity ECBilt-CLIO ([Opsteegh et al., 1998](#); [Goose and Fichfet, 1999](#)), which allowed the model ocean to actively respond to the prescribed calving and subsequent iceberg melt flux. Their findings can be summarized as follows: iceberg mass and melt distributions exhibit a gradient perpendicular to the coast with the maximum at the coast. Icebergs generally follow the ocean surface circulation, for instance drifting with the Weddell Gyre or forming an “iceberg alley” past Newfoundland. In the uncoupled model experiments iceberg trajectories reach 50°N from the north, and 50°S from the south (though only 3% of the icebergs pass 63°S ([Silva et al., 2006](#))), in the coupled runs they drift farther, reaching 40°N and 40°S in some places, respectively. The coupled experiments of [Jongma et al. \(2009\)](#) showed that the melt water from icebergs affects ocean salinity and temperature leading to an increase in Antarctic Bottom Water (AABW) formation of about 10% compared to a case with uniform calving flux redistribution. Finally, oceanic freshening and cooling due to iceberg melt increased the sea-ice area by 6–12% in these coupled experiments.

Uncoupled ice–ocean only models use salinity-restoring to avoid climatic drift but introduce the added disadvantage of damping the response to fresh-water forcing. Modern coupled models do not have this problem (few CGCMs still rely on flux-correction or salinity-restoring). However, coupled models are inherently more non-linear and teasing out the response of the climate system to a particular forcing is inherently difficult in the presence of

significant dynamic noise. For these reasons it is hard to anticipate whether the introduction of icebergs into a coupled model to better represent that part of the global fresh-water cycle will reproduce the significant response of an ice–ocean only model. The motivation for this study is thus threefold: first, to better close the fresh-water cycle in a comprehensive climate model in preparation for introducing interactive ice-shelf models; second, to fix the known bias, due to depositing frozen discharge into the coastal ocean in the absence of icebergs; and third, to assess the impact on the ocean of introducing interactive icebergs into the coupled system.

In this study we apply the iceberg model of [Bigg et al. \(1997\)](#) and [Gladstone et al. \(2001\)](#) to a new comprehensive CGCM, which was created at the GFDL. This coupled model system does not have an ice-sheet model but, as mentioned above, conveys excess snow to the coast. We will compare model results with and without the iceberg component. We will also compare our results with those of [Jongma et al. \(2009\)](#), who ran experiments with essentially the same iceberg model and with either the uniform redistribution approach applied only to the Southern Ocean south of 55°S or no calving flux at all for control experiments. The study presented here is the first that involves a full coupling of an iceberg model to a CGCM. In the absence of an explicit ice-shelf model, and hence without ice-shelf cavities, we feed the entire frozen fresh-water runoff into the iceberg model. In our coupled model the global calving rate amounts to 2200 Gt year<sup>−1</sup> on average, which compares well to the observational estimate of about 2300 Gt year<sup>−1</sup> ([Hooke, 2005](#)) justifying our approach. Like [Jongma et al. \(2009\)](#) our presentation of results focusses on the Southern Ocean for three reasons: first, about 90% of the global iceberg mass is located there; second, the impact of the newly included iceberg component is strongest in this region; and third, to improve comparability to previous studies.

We begin our study by introducing the model components, in particular highlighting changes we made to the iceberg model in order to improve the numerical stability and impact of the icebergs. In Section 3 we present the results of our model experiments, followed by the comparison to observational data and results of other model studies in Section 4. In the latter section, we also discuss shortcomings of the present model before concluding our study in Section 5.

## 2. The model

### 2.1. The coupled global circulation model

Our numerical experiments are conducted with the coupled global circulation model CM2G, which was developed at GFDL to be used as a contribution to the upcoming Intergovernmental Panel on Climate Change (IPCC) Fifth Assessment Report (AR5). This model includes components for atmosphere, land, ocean and sea-ice processes. The atmosphere and land models are AM2 and LM2, respectively, which have been used successfully in the CM2.0 and CM2.1 models (e.g. [Delworth et al., 2006](#)) and are presented in more detail in [Anderson et al. \(2004\)](#). Here, it is important to note that the local snow cover may not exceed 1 m in LM2. Any frozen precipitation in excess of this buffer is exported to the ocean with a river transport model. This calving flux only accounts for frozen runoff, though snow may melt and then contribute to the liquid runoff.

The main difference between the CM2.x models and CM2G is the ocean component which replaces the Modular Ocean Model (MOM) with a new code, internally referred to as Generalized Ocean Layer Dynamics (GOLD). GOLD is a descendent of the Hallberg Isopycnal Model (HIM) by [Hallberg \(1995\)](#), which fundamen-

tally differs from most ocean models in its vertical coordinate which are isopycnals in the interior. Some details of the new model can be found in Hallberg and Gnanadesikan (2006). An important detail for our study is that GOLD treats the fresh-water cycle directly, i.e. it does not use virtual salt fluxes to simulate fresh-water exchange to other model components.

The sea ice simulator (SIS) has multiple ice thickness categories and comprises the three-layer-thermodynamics of Winton (2000) including a prognostic snow cover. Sea-ice dynamics are based on the viscous–plastic rheology of Hibler (1979) and are solved with the elastic–viscous–plastic approach of Hunke and Dukowicz (1997). The sea ice is assumed to have a constant salinity of five.

We run the model on a global grid with a horizontal resolution of about  $1^\circ \times 1^\circ$  for ocean and sea ice and  $2^\circ \times 2.5^\circ$  for atmosphere and land. The atmospheric grid has 24 vertical levels and the oceanic 63.

This model setup is used to run a control experiment for comparison, which will be identified by CTRL in the following.

## 2.2. The iceberg model

The iceberg model is based on the works of Bigg et al. (1997) and Gladstone et al. (2001). Individual icebergs are simulated as Lagrangian particles in the Eulerian framework of the CGCM. In contrast to previous studies our iceberg model is fully embedded in the coupled system. We further developed the model, improving its robustness and added bergy bits in a separate experiment in order to study the effect of an extended iceberg life-time. For computational convenience the iceberg model is part of the sea-ice module SIS in CM2G. The full set of equations of the iceberg model is given in Appendix A.

### 2.2.1. Iceberg formation

Icebergs are land ice, i.e. consist of accumulated snow, and originate from ice shelves or glaciers. As the coupled model does not explicitly simulate ice sheets and ice shelves we use the snow discharge from land to generate icebergs. In LM2 snow that falls on land may accumulate to a maximum of one meter. Excessive snow mass is conveyed to the coast using a river network. In the control run the snow is simply deposited in the coastal ocean. With the introduction of the iceberg model we implemented a storage for frozen runoff in each coastal grid cell. The snow mass entering a coastal grid cell is split into ten iceberg size categories according to a statistical distribution (see Table 1), which follows the suggestion of Gladstone et al. (2001) and is based on ship observations. Whenever the critical mass of the individual category is exceeded, an iceberg is released. In order to reduce computational cost the smallest particles are clustered together, released in groups and modeled as a single entity (see Table 1 for mass scaling). Although the Lagrangian particles may represent several icebergs, the

thermodynamics of each iceberg in such a parcel is treated according to its original size. We simulate only icebergs with length scales of up to 2.2 km because we can assume that such small icebergs calve regularly (Schodlok et al., 2006). The calving storage is initialized with a random distribution avoiding a long spin-up of the climate simulation. New icebergs have a width to length ratio of 1:1.5 as suggested by Bigg et al. (1997), which is supported by observations (e.g. Jacka and Giles, 2007 and citations therein).

### 2.2.2. Iceberg drift and decay

In the model, iceberg drift is driven by drag by the atmosphere, sea ice and ocean as well as a wave radiation force. The momentum balance also includes Coriolis and pressure gradient forces. Three melting mechanisms describing iceberg ablation at or below the water line have been identified by Gladstone et al. (2001) to be of importance for the iceberg mass balance. This is influenced by the study of Løset (1993), which states that processes at the ice–air interface contribute only marginally to total iceberg ablation. The three mechanisms considered to be of importance are all described by empirical relationships. First, turbulence created by the difference of oceanic and iceberg motion leads to basal iceberg melt. The associated mass flux is derived proportional to this difference in motion, and the temperature difference between water and ice, where the iceberg is assumed to have a constant effective temperature of  $-4^\circ\text{C}$  (Løset, 1993). Second, we account for the effect of the buoyant convection along the sidewalls of the iceberg caused by the mentioned temperature contrast between iceberg and ocean. This melt flux is assumed to be solely a function of ocean temperature. A third relationship describes the impact of waves on the iceberg. In proportion to the sea state and the ocean surface temperature we estimate a melt and erosion rate that includes the excavating of the iceberg at the water line as well as the calving of overhanging slaps as a result of extensive excavation. Here, sea state is a direct fit to the Beaufort scale. Further details are given in Appendix A.

The simulated icebergs only interact directly with the ocean's surface layer. This does not take into account that icebergs of several hundred meter thickness reach into sub-surface layers. This shortcoming of the model is due to the implementation of the iceberg model in SIS forming a separate component in the coupled model system. Besides several advantages this includes the disadvantage that SIS only exchanges 2-D fields with the other model components.

Total energy in the CGCM is conserved because the iceberg parameterization is only used to spatially distribute the frozen fresh-water runoff from land. The iceberg “melt” flux is still returned as snow to the ocean model component as in CTRL and thus takes energy from the ocean to really melt, which leads to a cooling effect similar to real iceberg melt. In AM2/LM2 snow has a constant temperature of  $0^\circ\text{C}$ .

**Table 1**

Iceberg size categories with iceberg length and total thickness, mass levels, mass scaling factor and calving distribution. The mass scaling factor gives the number of icebergs represented by one Lagrangian parcel in the calculations of iceberg dynamics. The calving distribution divides the calving flux into the various iceberg size categories prescribing an iceberg size distribution at the calving site. Iceberg sizes and frequency distribution are as in Gladstone et al. (2001, their Table 2).

Category	Length (m)	Thickness (m)	Mass (kg)	Mass scaling	Calving distribution
1	60	40	$8.8 \cdot 10^7$	2000	0.24
2	100	67	$4.1 \cdot 10^8$	200	0.12
3	200	133	$3.3 \cdot 10^9$	50	0.15
4	350	175	$1.8 \cdot 10^{10}$	20	0.18
5	500	250	$3.8 \cdot 10^{10}$	10	0.12
6	700	250	$7.5 \cdot 10^{10}$	5	0.07
7	900	250	$1.2 \cdot 10^{11}$	2	0.03
8	1200	250	$2.2 \cdot 10^{11}$	1	0.03
9	1600	250	$3.9 \cdot 10^{11}$	1	0.03
10	2200	250	$7.4 \cdot 10^{11}$	1	0.02

### 2.2.3. Bergy bits

The relationships for iceberg melt are empirically derived and thus incorporate various subscale processes. It will be shown in Section 3.2 that the meltwater flux due to wave erosion dominates the fresh-water flux from icebergs. As described above, the wave erosion function does not only account for melting of ice at the iceberg's surface but also for a partial break-up of the iceberg. Thus, wave erosion actually leads to the formation of small child icebergs, so-called bergy bits. These bergy bits are blocks of still solid ice and not liquid fresh water. As the ratio of liquid to solid mass flux is unclear for the wave erosion function, we carried out two experiments, one in which all wave erosion flux becomes liquid instantly (experiment BERG) as in the original iceberg model, and one in which the entire wave erosion mass flux is used to form solid bergy bits (BITS). The bergy bits are assumed to travel with their parent iceberg and melt according to the remaining two melt functions for basal and side wall melt. The World Meteorological Organization (WMO) describes bergy bits as “large pieces of floating glacier ice, generally showing less than 5 m above sea level but more than 1 m and normally about 100–300 m<sup>2</sup> in area” (WMO, 1989). In our model bergy bits are initialized as cubes with a side length of 40 m or less, not exceeding their parent iceberg's shortest dimension.

## 3. Results

### 3.1. Calving

The global calving flux available to iceberg formation in the CGCM amounts to a long term, 100 year average of 2210 Gt year<sup>-1</sup>. This mass flux is robust across all our model experiments, varying only by 10 Gt year<sup>-1</sup>. The standard deviation, which indicates inter-annual variability, is 130 Gt year<sup>-1</sup> with a maximum difference of 10 Gt year<sup>-1</sup> between the experiments. Fig. 1a depicts the time series of experiment BERG (black line). The time series is dominated by inter-annual variations, multi-annual or decadal cycles are very weak. The global calving rate is dominated by the discharge from Antarctica, which amounts to  $2000 \pm 130$  Gt year<sup>-1</sup> in our experiments. In the northern hemisphere, runoff from

Greenland is largest with  $210 \pm 40$  Gt year<sup>-1</sup>. Further, marginal contributions of less than 1 Gt year<sup>-1</sup> in total originate from, for instance, Alaskan and Himalayan glaciers.

On the southern hemisphere major snow discharge and therefore iceberg calving sites in the model are located in the Ross (150–200°W) and Amundsen seas (95–120°W) as well as in the southwest of the Weddell Sea (10–60°W). Discharge into the Davis Sea region (80–110°E) is an order of magnitude smaller though still notable. About two thirds of all coastal grid cells around Antarctica have a calving flux of more than 1 Gt year<sup>-1</sup>.

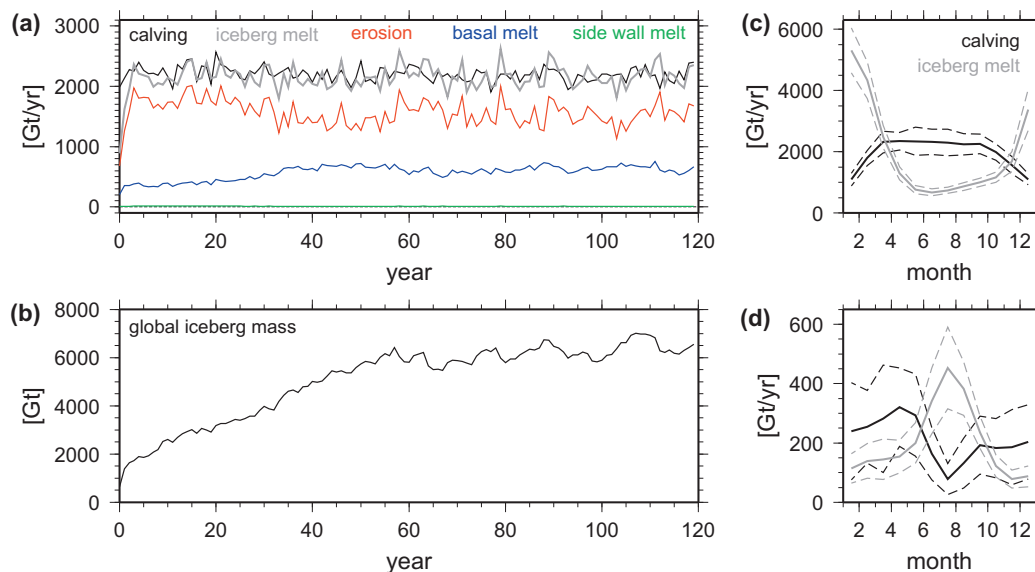
In contrast, only one-third of the Greenlandic coastal grid cells have a significant calving flux. Important discharge sites are along the southeast coast and in the Disko Bay region (~70°N, 55°W).

Fig. 1c and d depicts the seasonal cycle of calving in the southern and northern hemispheres respectively. The frozen fresh-water discharge is directly linked to the precipitation having only a time lag of order 10 days at maximum. The discharge rate from Antarctica is high during the winter months April to September when the snow cover of the continent is less exposed to solar radiation and warm temperatures causing surface melt. Though precipitation over Antarctica is greater during summer, the snow quickly melts and becomes liquid runoff during this season, and hence does not affect iceberg calving. In the northern hemisphere maximum calving occurs in April at the end of the winter season.

### 3.2. Icebergs

The iceberg mass accumulated on the ocean reaches its equilibrium after about 60 years (see Fig. 1b), which means iceberg melt does not fully balance calving in the first 60 years of our experiments, though the meltwater flux reaches the same order of magnitude as calving already after 5 years (Fig. 1a). In the equilibrium state roughly 100,000 individual icebergs are continuously present in the simulation. This number represents the dynamically active Lagrangian parcels and does not incorporate the mass scaling factor.

In Fig. 1a the time series of the meltwater flux is presented together with its three components: the fluxes due to wave erosion, basal melt and side wall convection. With a global rate of 1550 Gt year<sup>-1</sup> (averaged over years 60–120) the wave erosion flux



**Fig. 1.** Results of experiment BERG. (a) Time series of modeled calving flux (black) and iceberg melt rate (gray). The partitioning of the melt flux is depicted in red for wave erosion, blue for basal melt and green for side wall melt. (b) Time series of global iceberg mass accumulated on the ocean. (c) Mean annual cycle of calving (black) and iceberg melt (gray) for the southern hemisphere. (d) same as panel c but for the northern hemisphere. Dashed lines mark plus/minus one standard deviation of the mean. (For interpretation of the references to color in this figure legend, the reader is referred to the web version of this article.)



is clearly the largest contributor accounting for 70% of the total melt flux. It is 2.5 times greater than the basal melt flux on global average. The contribution by side wall melt does not exceed  $17.5 \text{ Gt year}^{-1}$  and is thus almost negligible. The wave erosion flux also has the strongest inter-annual variations with amplitudes of up to  $630 \text{ Gt year}^{-1}$ .

Iceberg melt has a maximum in January and July on the southern and the northern hemisphere, respectively (Fig. 1c and d). In contrast to the maximum of the calving flux the peak of iceberg melt is much more pronounced because iceberg mass accumulates during winter and quickly melts when the sea-ice cover retreats and ocean temperatures rise. Sea ice plays an important role here as it insulates the ocean from the atmosphere hindering radiative warming of the ocean surface and momentum exchange, which both are important for the wave erosion to develop its full effect. In the CTRL run, with the absence of icebergs, the two processes of calving (i.e. snow discharge and fresh-water release to the ocean) appear as one, which imposes a false timing for the melt of the frozen discharge. As shown in Fig. 1 calving and fresh-water release to the ocean have opposite annual cycles. By introducing

icebergs and a storage for the calving flux at the coast these two processes are decoupled and have shifted the fresh-water release correctly towards summer.

The spatial distribution of the meltwater flux depicted in Fig. 2, which shows results of BERG, is very similar to the mass distribution of icebergs (not shown). The meltwater flux has a strong gradient perpendicular to the coast, which is most prominent in the Southern Ocean. This agrees well with the model results of Gladstone et al. (2001) and observational records (Jacka and Giles, 2007). The maximum melt flux of up to  $10^3 \text{ mm year}^{-1}$  is located near the coast, where many of the small icebergs accumulate during the winter and quickly decay in the subsequent summer season. For larger icebergs two major export routes can be identified in the Southern Ocean. The overall largest export is found in the western Weddell Sea where icebergs follow the persistent gyre so that melt rates reach  $10^{2.5} \text{ mm year}^{-1}$  far off the coast. The second largest export area is fed from the western Ross Sea region and melt rates north of the Ross Sea exceed  $10^{1.5} \text{ mm year}^{-1}$ . In these two regions and additionally southwest of Australia icebergs penetrate far north. Large icebergs can reach latitudes of  $40^\circ\text{S}$  in the

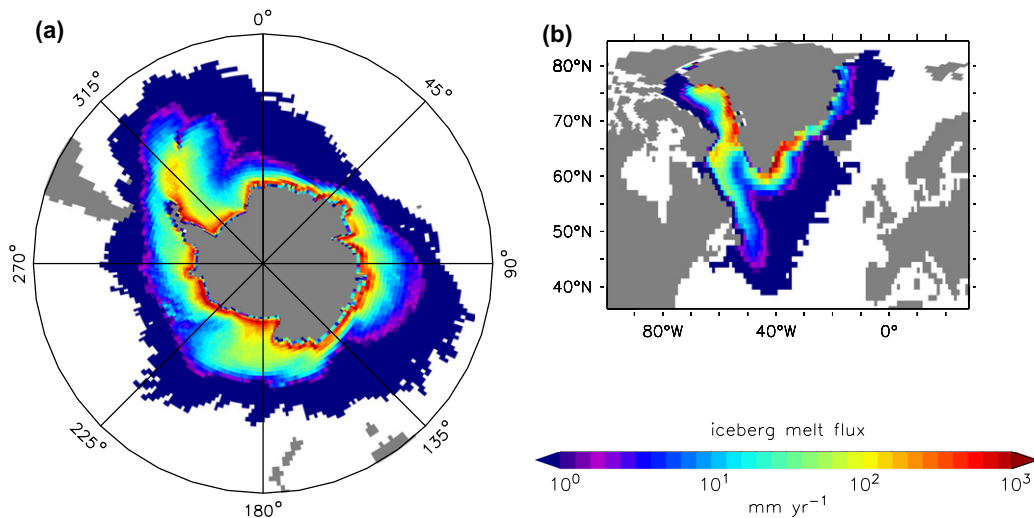


**Fig. 2.** Hundred year average of the fresh-water flux to the ocean in  $\text{mm year}^{-1}$  from iceberg melt in experiment BERG for icebergs originating from (a) Antarctica and (b) Greenland. Note the use of a logarithmic color scale. The irregular outline is a consequence of the passage of individual large icebergs.

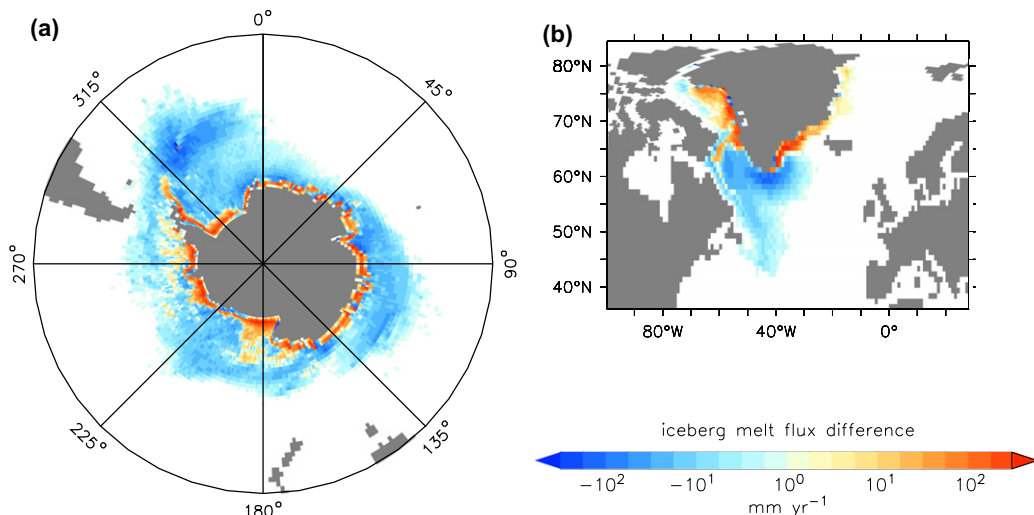


**Fig. 3.** Difference BERG-BITS of the fresh-water flux due to iceberg melt in  $\text{mm year}^{-1}$  for (a) the Southern Ocean and (b) the North Atlantic derived from 100 year averages of the two experiments. Blue colors indicate a greater iceberg melt water flux to the ocean in BITS than in BERG, red indicates a smaller flux in BITS.

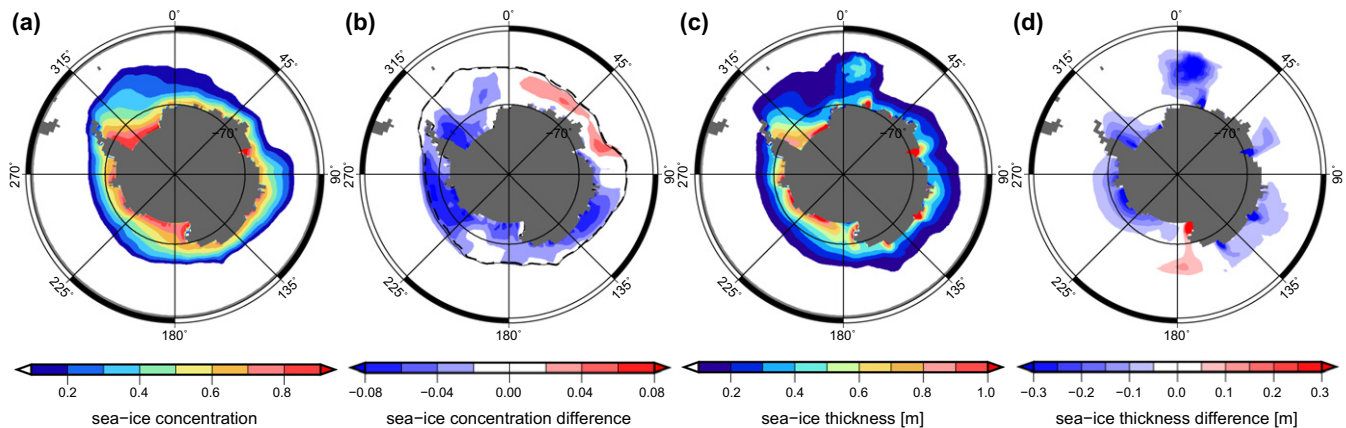


**Fig. 4.** Hundred year averages of sea-ice properties and their change due to the introduction of icebergs. (a) Sea-ice concentration in CTRL. (b) Concentration difference of BITS-CTRL. (c) In situ sea-ice thickness in m in CTRL. (d) Thickness difference in m of BITS-CTRL.

Pacific sector and even 30°S in the Atlantic and Indian Ocean sectors. East of Greenland icebergs follow the East Greenland Current around the southern tip entering the Labrador Sea from the east (Fig. 2b). Icebergs coming from the Baffin Bay enter the Labrador Sea from the north to form the famous iceberg alley passing Newfoundland and penetrating into the North Atlantic as far south as 40°N (Fig. 2b).

Although the above major features of the spatial distribution of icebergs are very similar in both experiments, BERG and BITS, the introduction of the bergy bits reduces the fresh-water input close to the coast by up to  $10^{2.5}$  mm year<sup>-1</sup> (Fig. 3), which is close to the magnitude of the total flux (Fig. 2). The bergy bits delay the meltwater discharge to the ocean while they drift with their parent iceberg. This causes a wider distribution of the fresh-water input farther out at sea, where the flux in the BITS run exceeds those in the BERG experiment by up to  $10^2$  mm year<sup>-1</sup> (Fig. 3). This promotes the effect of the icebergs as will be shown in Section 3.4.

### 3.3. Sea ice

The introduction of icebergs lead to a reduction in sea-ice compactness and thickness in particular in the Southern Ocean. These changes are shown in Fig. 4 as differences between the BITS and CTRL experiments along with the sea-ice concentration and thickness of the CTRL run. While the long-term mean position of the sea-ice edge in the Southern Ocean has only changed marginally, the fractional coverage is strongly reduced in about three-quarters of the sea ice covered area (Fig. 4b). This means a loss of about  $0.5 \times 10^6$  km<sup>2</sup> of sea-ice cover. The strongest decrease in sea-ice concentration of 6–8% is found in the Amundsen, Bellinghausen (70–95°W), Weddell, and D'Urville seas (110–150°E), i.e. along the major export routes of icebergs mentioned above. In these sectors the mean sea-ice extent has slightly decreased. In contrast, an increase in sea-ice concentration of up to 6% and a slightly greater extent is visible between 0° and 90°E. This increase in sea-ice area is associated with extensive iceberg melt occurring locally and further upstream of the Antarctic Coastal Current. The related changes in sea surface salinity (SST) are discussed below.

Changes in in situ sea-ice thickness are less extensive than changes in sea-ice concentration. Compared to the CTRL experiment sea ice is thinner in the BITS run mostly in places close to major, single discharge points. For example, a plume of thinner sea ice is visible extending from Prydz Bay (75°E), where the Amery Ice Shelf is located (Fig. 4d); the same can be seen for major discharge

points in the D'Urville Sea or the Haakon VII Sea (0–30°E). In the latter, the decrease in thickness is most pronounced with about 0.5 m. More widely spread decreases in sea-ice thickness can also be found in the Weddell, Amundsen, and Bellinghausen seas (Fig. 4d). The spreading is caused by a chain of discharge locations along the coast in the respective region.

In the CTRL run, sea ice of extraordinary thickness grows in small (in terms of the 1° resolution of the model grid) semi-enclosed bays because huge amounts of frazil ice are formed when the snow discharge enters an ocean at the freezing point. Since snow is fresh water and model sea ice has a constant salinity of five salt is taken from ambient ocean waters during the formation. Fig. 5 depicts the difference in salt uptake by sea ice between runs CTRL and BITS. We can clearly see the discrete snow discharge locations around Antarctica represented by positive differences in Fig. 5. The effect is less prominent around Greenland because the discharge volume amounts to only 10% of that of Antarctica. The introduction of icebergs successfully eliminates this false freshening signal in the ocean.

In the BITS experiment a sea-ice thickness increase of 0.5 m based on a 100 year average can be seen in the western Ross Sea (Fig. 4d). This can be explained by an accumulation of icebergs in the western corner of the Ross Sea, driven by predominantly on-shore and circular wind and ocean current patterns, respectively. Their local melt in summer produces a fresh-water lens that initiates stronger sea-ice growth.

In contrast, changes of the sea-ice cover due to the introduction of icebergs are small and local on the northern hemisphere. At the major calving sites along the southeast and west coast of Greenland sea-ice concentration is reduced by up to 10% right at the coast. A significant change in sea-ice thickness was not found on the northern hemisphere.

The decrease in sea-ice mass between the control run and those with icebergs is mainly caused by the redirection of the snow discharge mass. In the CTRL experiment the sea-ice cover benefits from discharging the calving flux right at the coast in winter. The instantaneous frazil formation results in a generally thicker and denser sea-ice cover. A simple calculation based on the scales of the involved mass flux and sea-ice area gives a rough estimate of the impact of redirecting the calving flux: the snow discharge from Antarctica is about  $2 \cdot 10^{15}$  kg year<sup>-1</sup>. Distributing this mass over the entire southern hemisphere sea-ice area, which is of the order of  $10^{13}$  m<sup>2</sup>, and assuming a sea-ice density of 900 kg m<sup>-3</sup> yields a sea-ice thickness decrease of 0.22 m year<sup>-1</sup>. This corresponds to an energy uptake of 2.2 W m<sup>-2</sup> (the latent heat of fusion of water is  $334 \cdot 10^3$  J kg<sup>-1</sup>). For comparison, in a climate scenario with

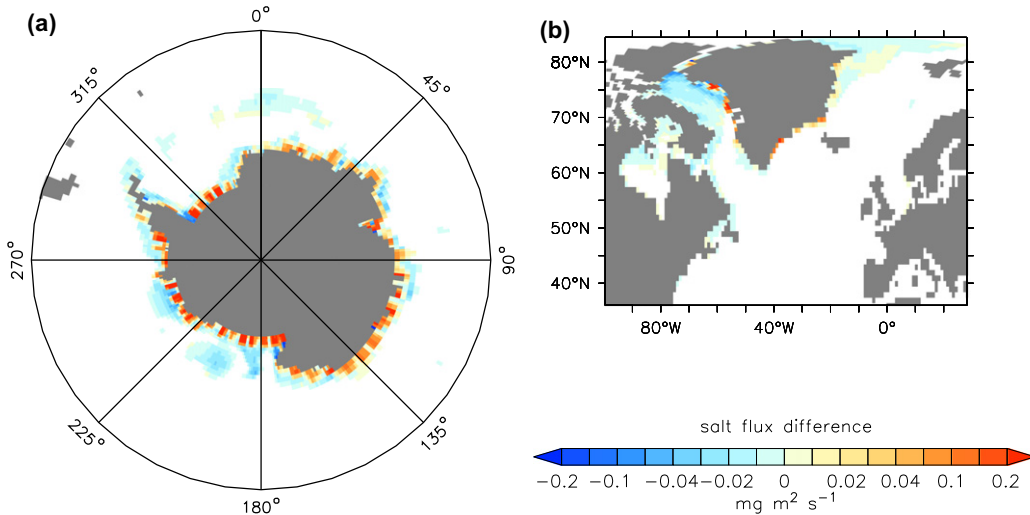


**Fig. 5.** Difference CTRL-BITS of the salt flux from the ocean into sea ice in  $10^{-6} \text{ kg m}^{-2} \text{ s}^{-1}$  for (a) the Southern Ocean and (b) the North Atlantic based on a 100 year mean. This salt flux is associated with frazil ice formation. Yellow-red colors (positive values) indicate less sea-ice formation in BITS due to redirecting the calving flux which ultimately lead to local sea-ice formation in CTRL, blue colors (negative values) mean more sea-ice formation in BITS where freshening and cooling now prevail due to iceberg melt farther off shore.

doubled atmospheric  $\text{CO}_2$  the global radiative forcing is about  $4 \text{ W m}^{-2}$  (Meehl et al., 2007, Table 10.2).

### 3.4. Ocean

#### 3.4.1. Surface properties

The reduced sea-ice concentration in the experiments with icebergs results in a warming of the ocean due to greater radiative absorption leading to an increase of SST (see Fig. 6). This summer effect dominates the presented annual mean SST over any sea-ice mass gain from enhanced freezing during winter. The warming of the ocean surface is most prominent in the Pacific sector of the Southern Ocean with an increase of up to  $0.5^\circ\text{C}$ . Its center is roughly located at the sea-ice edge (cf. Figs. 4b and 6b). In contrast, a few locations with slight cooling can be found in the Atlantic and western Indian Ocean sectors. The warming and cooling patterns correlate with the distribution of sea-ice concentration decrease and increase, respectively, depicted in Fig. 4b.

The differences in the sea surface salinity (SSS) between the CTRL and BITS experiments is more diverse. The magnitudes of freshening and salinization are the same with values of up to 0.2.

Surface waters become more saline in the Amundsen and Bellinghausen seas, and in the D'Urville Sea. A wide area of freshening is located in the Atlantic and Indian Ocean sectors. Also the Ross Sea area is fresher in the BITS run. Here, the fresh-water lens addressed earlier in conjunction with the sea-ice thickness changes is visible (dark blue spot in the very southwestern corner of the Ross Sea in Fig. 6d) with an overall extreme difference of  $-1.37$  at  $74.2^\circ\text{S}$ . In general, changes in salinity can be attributed to the changed spatial distribution of frozen fresh-water discharge to the ocean in the iceberg experiments. However, mechanisms leading to changes in SSS are complex and involve ocean circulation and sea-ice melt, too. For instance, the ocean is saltier in BITS where a large calving flux initiates frazil-ice growth in CTRL, which is associated with a reduction of the ocean salinity because the calving flux is fresh and sea ice has an assigned constant salinity in the CGCM (Fig. 6). The reduction in sea-ice mass due to a redirected calving flux results in a reduced fresh-water input to the ocean from sea-ice melt leading to greater SSS in BITS (cf. Figs. 4d and 6d around  $0^\circ$  longitude). The widespread freshening in BITS in the Atlantic and Indian Ocean sectors, which stimulates sea-ice growth (Fig. 4b), originates from an accumulation of iceberg melt water

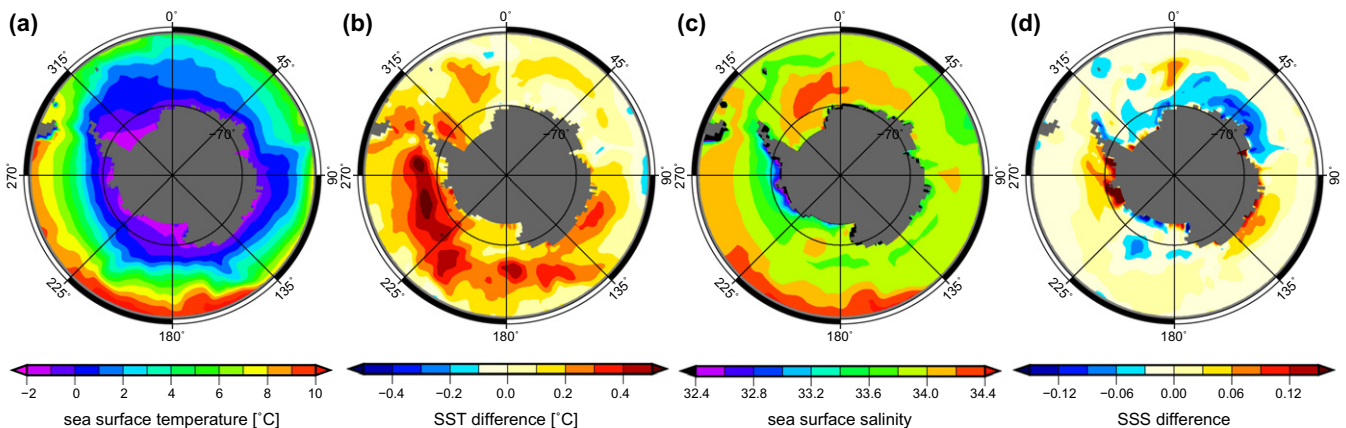


**Fig. 6.** Hundred year averages of sea surface properties and their change due to the introduction of icebergs. (a) Sea surface temperature (SST) in  $^\circ\text{C}$  in CTRL. (b) SST difference in  $^\circ\text{C}$  of BITS-CTRL. (c) Sea surface salinity (SSS) in CTRL. (d) SSS difference of BITS-CTRL.

in this region. This is favored by a strong southward component of the Antarctic Coastal Current in this region (not shown) and major calving sites upstream, such as the Amery Ice Shelf.

### 3.4.2. Deep convection

In the CTRL experiment the snow discharge enters the ocean directly at the coast while in the BERG and BITS experiments icebergs transport this fresh water away from the coast. Exporting this fresh water off the continental-shelf regions enhances the formation of dense waters in these areas, which in turn encourages deep convection at the shelf break in particular in the Weddell and Ross seas. The resulting increase in downslope flow at the shelf break is visualized in Fig. 7 in terms of the CFC-11 tracer concentration. Along the shelf break in the Weddell Sea and west of the Ross Sea the CFC-11 concentration is up to  $1 \times 10^{-9} \text{ mol kg}^{-1}$  higher in BITS compared to CTRL at a depth of about 3000 m 31 years after the tracer has been released at the surface in model year 89. This is

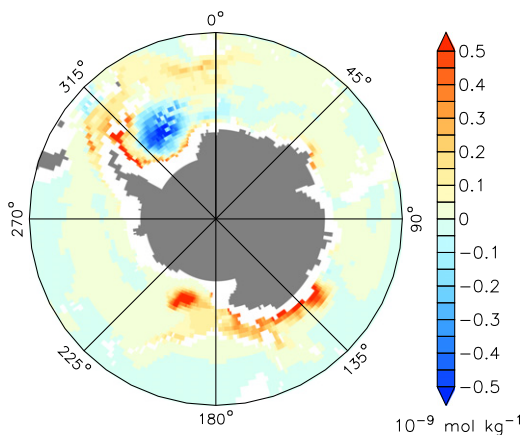


**Fig. 7.** Annual average of the CFC-11 concentration differences BITS-CTRL in  $\text{mol kg}^{-1}$  in the Southern Ocean at 3000 m depth of model year 120, 31 years after tracer release at the surface. The CFC tracer emphasizes continental-shelf convection in the Weddell and Ross seas, which are strongly increased in the iceberg experiments (positive differences). The impact of an event of strong open ocean convection in the Weddell Sea in CTRL can also be seen (negative differences). Regions of water depths of less than 3000 m are white.

an increase by a factor of 2–3. At this time the CFC-11 concentration reaches  $1 - 1.5 \times 10^{-9} \text{ mol kg}^{-1}$  along the shelf break in the BITS experiment (not shown). Fig. 7 also depicts the effect of an event of strong open ocean convection in CTRL in the central Weddell Sea. Due to the deep mixing the CFC-11 concentration is up to  $0.5 \times 10^{-9} \text{ mol kg}^{-1}$  greater than in BITS, where it amounts to only  $0.1 \times 10^{-9} \text{ mol kg}^{-1}$ .

The enhanced ventilation of deep waters with the help of icebergs can also be deduced from an ideal age tracer, which simply counts the years since the last contact of water masses with the ocean surface. Fig. 8 shows the results of all three experiments for the Atlantic Ocean at a depth of 4200 m. To begin with, we demonstrate the effect of the icebergs by comparing the spatial extent of the 70 year isochrone (yellow in Fig. 8). In BERG the younger waters reach farther north and east from the Weddell Sea than in CTRL, reaching  $39^\circ\text{S}$  and  $8^\circ\text{E}$ , respectively, compared to only  $47^\circ\text{S}$  and  $5^\circ\text{W}$ , respectively. In BITS this extent is not much increased but waters are much younger. Apart from the strong effect of the open ocean convection in CTRL mentioned above, the water age does not fall below 50 years in CTRL and BERG in the South Atlantic, whereas BITS results in waters younger than 30 years at this depth. This emphasizes the importance of transporting the calving flux away from coastal and shelf regions, in which the additional bergy bits are obviously more effective.

Although the open ocean convection in CTRL also allowed waters younger than 40 years to penetrate to greater depth in the central Weddell Sea (Fig. 8a) it is important to enable CGCMs to produce deep waters on the continental shelf. This process, also referred to as the continental-shelf pump, is expected to have a stronger impact on the carbon budget of the climate system than open ocean convection (Tsunogai et al., 1999). Carbon solubility depends strongly on the temperature of the water. On shallow shelves the water can cool down much more than in the open ocean and hence dissolve more  $\text{CO}_2$ . Additionally, the residence time at the surface of water on the shelf is longer, which also allows an increased uptake of carbon compared to the open ocean. The release of oxygen to the atmosphere happens much faster than the uptake of carbon. Hence, water originating from shelf convection has a greater carbon to oxygen ratio than water from open ocean convection. Considering the estimate of Tsunogai et al. (1999) we conclude that it is important to simulate the convection

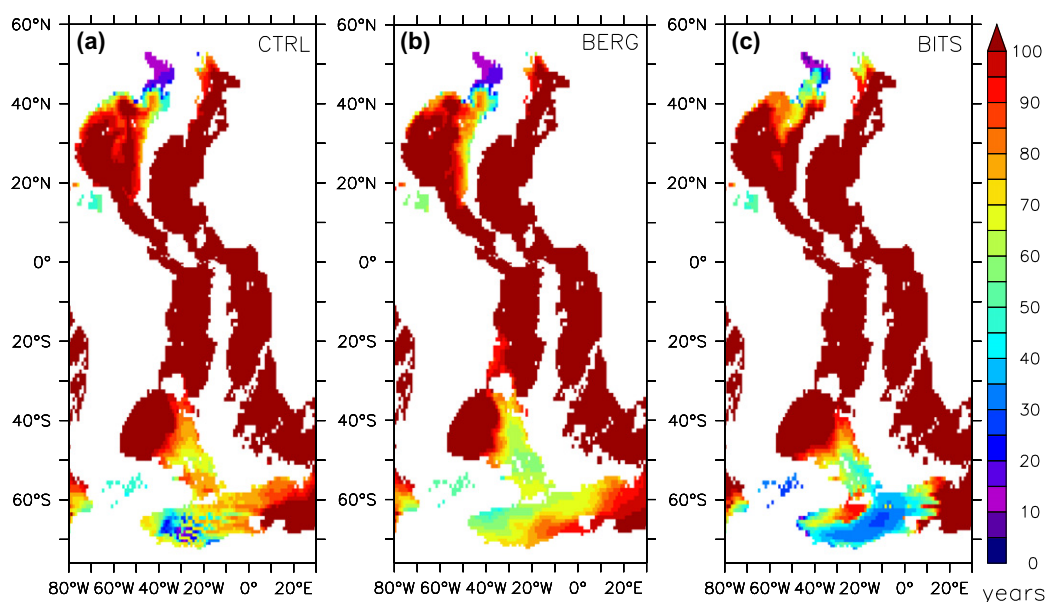


**Fig. 8.** Ideal age tracer of ocean waters in the Atlantic Ocean at 4200 m depth in years for (a) CTRL, (b) BERG, and (c) BITS. The annual average of model year 120 is shown.



mechanisms correctly in a CGCM, which is used for ecosystem studies. The icebergs, and in particular the bergy bits, help to strengthen the continental shelf pump.

Comparing the CTRL and BERG results in Fig. 8a and b, respectively, the icebergs seem to have less impact on the age structure of the deep water in the North Atlantic but result in an increase in the amount of younger waters, which are less than 70 years old. It is noteworthy that the pathway of the deep water changes in the BITS experiment (Fig. 8c), which no longer flows along the Mid Atlantic Ridge but heads southward in the center of the basin.

## 4. Discussion

### 4.1. Comparison to previous model studies and observations

A correctly simulated calving flux is a necessary precondition in order to achieve a natural distribution of iceberg mass on the ocean. In the absence of an ice-shelf model we use the snow discharge generated by the CGCM as input for the iceberg simulation. Observational estimates of the calving flux have a rather wide range. Jacobs et al. (1992) list estimates of nine different studies, including their own, ranging from 855 to 2400 Gt year<sup>-1</sup>, averaging at 1753 Gt year<sup>-1</sup> for Antarctica. Gladstone et al. (2001) made a very comprehensive approach to provide a climatological calving rate of 1332 Gt year<sup>-1</sup> for their iceberg model study. More recently Hooke (2005) stated a calving flux of  $2072 \pm 304$  Gt year<sup>-1</sup> for Antarctica and  $235 \pm 33$  Gt year<sup>-1</sup> for Greenland. For their model study Bigg et al. (1997) derived a mass flux of 218 Gt year<sup>-1</sup> from Greenland. And most recently Rignot and Kanagaratnam (2006) calculated Greenlandic glacier flow speeds from remote sensing data yielding a calving rate of 291 Gt year<sup>-1</sup>. A source of uncertainty, in particular for the Antarctic, is the unknown ratio of ice-shelf bottom melt and calving. Both play an important role in the mass balance of the Antarctic ice sheet and their ratio differs from site to site (Lemke et al., 2007). Within these limits the agreement of our modeled and the observed calving fluxes is very good. The Greenlandic calving flux in our model amounts to 210 Gt year<sup>-1</sup>. Here, it should be kept in mind that Rignot and Kanagaratnam (2006) account for the recent increase in flow speed of the glaciers, i.e. our model better matches a climatological mean. With an average calving rate of 2000 Gt year<sup>-1</sup> from Antarctica our model is close to the average calving estimates (Jacobs et al., 1992; Hooke, 2005) but produces 50% more iceberg mass per year than

Gladstone et al. (2001) prescribed in their model study. This needs to be considered when comparing the melt water distribution in the Southern Ocean to Gladstone et al. (2001) and Silva et al. (2006).

Iceberg calving rate estimates at individual locations are provided by Gladstone et al. (2001) and Rignot and Kanagaratnam (2006) for Antarctica and Greenland, respectively. In Fig. 9 we present the calving flux from the BERG experiment averaged over 100 years together with these data. Our model has 88 discharge points around Antarctica but Gladstone et al. (2001) chose only 29 calving sites. For this comparison, not for the experiments, we concentrated the modeled flux at the locations of Gladstone et al. (2001) combining catchment basins of the model to resemble those of the observations. We also merged the data of 32 individual Greenlandic glaciers given by Rignot and Kanagaratnam (2006) and the 24 discharge locations around Greenland of the CGCM into 9 calving sites to achieve best overlap of the catchment basins and pronounce the major iceberg formation areas. From the maps in Fig. 9 we can see that the calving flux in our simulations has a realistic spatial distribution, i.e. there are distinct maxima at locations of large ice shelves and glaciers around Antarctica and Greenland, respectively. The difference in total calving between Gladstone et al. (2001) and our model is mostly due to an overestimation by the model in the Ross, Amundsen, and Bellinghausen seas (Fig. 9a). In a future version of the CGCM this could be changed by dividing the snow discharge between calving and ice-shelf bottom melt. Ice-shelf bottom melt is particularly strong in the Amundsen and Bellinghausen seas (Rignot and Jacobs, 2002). In the case of Greenland the spatial distribution of the simulated calving flux compares well with the observations of Rignot and Kanagaratnam (2006), in particular along the west coast of Greenland (Fig. 9b).

It is important to note that the major impact of the icebergs on the coupled system is the effective transport of fresh water away from the shelf regions. As Fig. 10a shows, iceberg melt water rarely accounts for more than 10% of the total fresh-water input to the open ocean in our experiments, i.e. the fresh water released by the icebergs barely affects the ocean's stratification in these regions. In contrast, in coastal areas iceberg melt accounts for up to half of the fresh-water input. Hence, large icebergs that survive several melt seasons and drift farther away from the coast have the greatest impact on the fresh-water balance. In contrast, a transport of the calving flux with sea ice, as apparently happens in CTRL,

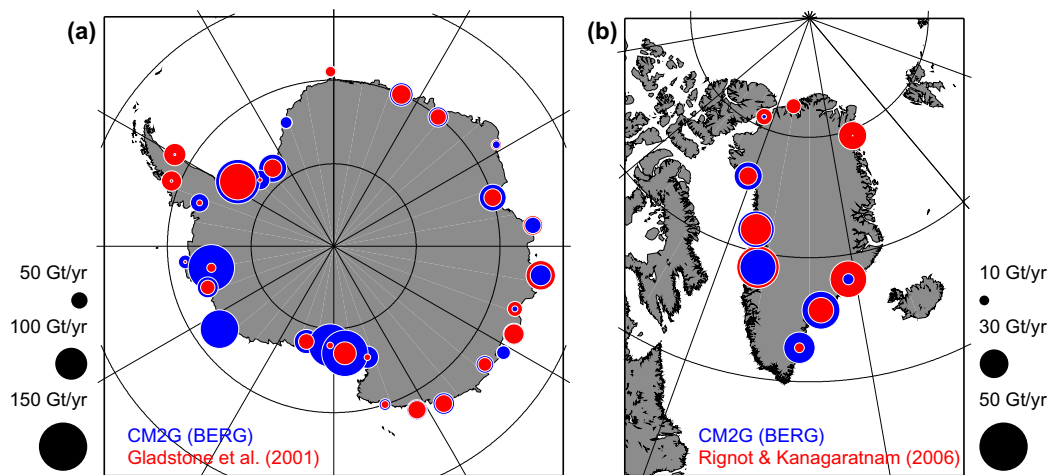


**Fig. 9.** Comparison of simulated (blue, from experiment BERG) and observed calving rates (red). (a) Twenty-nine calving locations around Antarctica given by Gladstone et al. (2001). (b) Glacial discharge published by Rignot and Kanagaratnam (2006) concentrated in nine main regions. (For interpretation of the references to colour in this figure legend, the reader is referred to the web version of this article.)

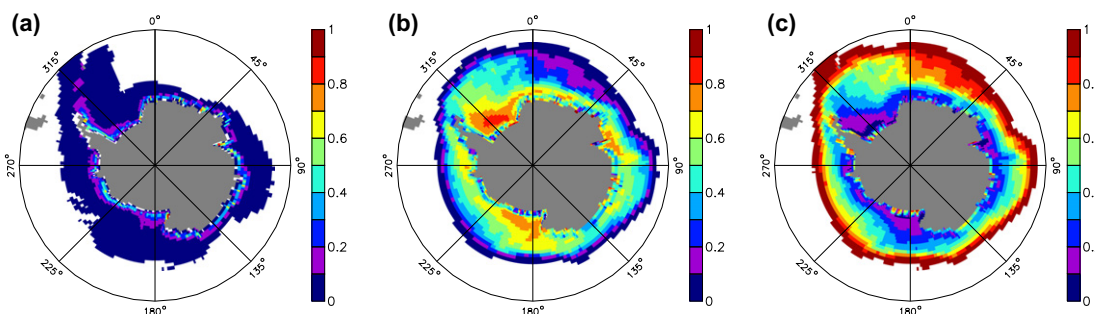


**Fig. 10.** Partitioning of the fresh-water flux entering the Southern Ocean: (a) fraction of iceberg melt, (b) fraction of sea-ice melt, and (c) fraction of precipitation including liquid runoff. Results of the BITS experiment are shown. In panels a and b white areas indicate values falling below 0.005, in panel c this marks values greater than 0.995.

where the snow is quickly turned into frazil ice and further enhancing sea-ice thickness, is less effective, because sea-ice melt dominates the fresh-water flux into the ocean in particular on the continental shelves in the Weddell and Ross seas (Fig. 10b). Silva et al. (2006) estimated that about half of the total meltwater flux from icebergs in the Southern Ocean is related to giant icebergs, icebergs that exceed 8 km in length, which are not yet considered in our model. The authors also showed that these giant icebergs can reach farther north than those we simulate here. Gladstone et al. (2001) found that iceberg melt rarely reaches the same magnitude as precipitation but does so for instance in coastal areas in the Weddell Sea, which agrees with our results (Fig. 10a and c).

Forming icebergs from the snow discharge has a strong impact on the compactness and thickness of the sea-ice cover in the Southern Ocean. However, the simulated sea-ice extent (total area within the 15% isoline) is mostly unaffected (Fig. 4b). With  $15.3 \times 10^6 \text{ km}^2$  the model's sea-ice extent exceeds the observed long-term (1979–2006) average of  $11.5 \times 10^6 \text{ km}^2$  (Cavalieri and Parkinson, 2008) by one-third. In contrast, the simulated mean sea-ice area, which considers the fractional area covered by sea ice, is smaller ranging between  $7.0 \times 10^6 \text{ km}^2$  (BERG and BITS) and  $7.4 \times 10^6 \text{ km}^2$  (CTRL) compared to the observed  $8.7 \times 10^6 \text{ km}^2$  (Cavalieri and Parkinson, 2008). This clearly shows the low compactness of the southern hemisphere sea ice in our CGCM results. Furthermore, the annual mean sea-ice thickness is too thin. In the CTRL experiment, which has generally thicker sea ice than the runs with icebergs, the ice is about 0.2–0.5 m thinner than observed (Worby et al., 2008) in many locations, in particular (far) off the coast. The underestimation is greater in those regions where thicker ice occurs in both, model and data. The simulated sea-ice cover of the CTRL experiment is thicker than observed where ice growth is forced by the snow discharge from land. The smaller sea-ice mass in our model can be attributed to the generally warmer surface ocean south of  $50^\circ\text{S}$ . The CTRL run has a SST warm bias of about  $2^\circ\text{C}$  on average in this region (results shown in Fig. 6a compared to a 20 year composite of observed SST from Reynolds et al. (2002)). Discharging snow in winter and hence into a cold ocean in the CTRL experiment results in an extensive frazil-ice formation, which makes the sea ice more resistive to melting by significantly increasing its thickness (see above) and hence partly compensates the impact of warm SSTs. We found that enhanced growth in winter, as a result of a generally thinner and less compact sea-ice cover in experiments BERG and BITS, cannot compensate for the additional melt in summer caused by a reduction in surface albedo due to the same sea ice changes. In summer the ocean gains more heat due to open water areas within the ice cover enhancing the warm bias the model has in the Southern Ocean (Fig. 6b).

The reduced compactness of the sea-ice cover in the experiments with icebergs unintentionally affects the life-time of the icebergs. The dominant iceberg melt parametrization, the wave

erosion, is moderated by sea-ice concentration because the ice cover damps waves. The changes in sea ice between runs with icebergs and without are mainly a result of the redirection of the snow discharge and to a lesser degree due to the meltwater distribution of the icebergs.

In general, the effect of icebergs in a CGCM strongly depends on how the control run deals with the excess snow runoff. While the runoff enters the ocean directly at the coast in CTRL, Jongma et al. (2009) chose the opposite approach: a homogeneous redistribution to the Ocean south of  $55^\circ\text{S}$ . As we mentioned in the introduction they performed a similar study but prescribed the calving flux. In Jongma et al. (2009) the additional fresh water in polar waters from iceberg melt enhances stratification which in turn stimulates sea-ice formation. The authors also found an increase in the production of AABW of 1–2 Sv due to the freshening and cooling effect of iceberg melt. In our experiments BERG and BITS the AABW production is greater than in CTRL by 1 Sv at  $60^\circ\text{S}$ . This change is about 10% of the total AABW production in CTRL, which also agrees well with the results of Jongma et al. (2009).

The snow discharge from the continents may be small compared to other sources of fresh water entering the ocean, but where and when the calving flux enters the ocean matters. It should be noted here, that in all our experiments the liquid runoff is greater than the snow discharge throughout the year, which means that the ability of the icebergs to reduce the fresh-water bias in coastal waters, in particular around Antarctica, is limited. In order to reduce computational costs the explicit iceberg simulation could be replaced by an invariant distribution pattern. This distribution could be derived from a long-term average, e.g. over 100 years, of the iceberg melt water distribution of experiments such as BERG or BITS. This approach is along the lines of Gordon et al. (2000) but would improve the redistribution pattern to match the individual CGCM's climate and climate change response. Applying the iceberg melt water pattern could also change the results of so-called waterhosing experiments because the typically used release pattern of the additional fresh water differs from that of iceberg melt presented here (cf. Fig. 2 with Gerdes et al. (2006, Fig. 3) or Stammer (2008, Fig. 1)).

#### 4.2. Shortcomings of the current model

The iceberg model we use in this study has certain shortcomings, which are partly due to simplifications that were necessary to realize this study with the CGCM CM2G and partly caused by limited knowledge on related processes in nature. In the following we will briefly discuss most of these issues. For all of these we seek solutions, but the time scale is beyond this study. The expected impact of the various missing processes on the CGCM result differs.

Currently iceberg calving is initiated by splitting the snow discharge into ten iceberg size categories. There are two caveats regarding this step function, which we adopted from Gladstone

et al. (2001): first, the first bin is the major mode of the distribution (see last column of Table 1) and represents all icebergs that are smaller than 60 m in length, i.e. they are of the same size as our bergy bits. This means that the first bin of the distribution includes brash ice, which should not be considered an iceberg but can be assumed to melt locally or be enclosed by sea ice. We conclude that the initial length of icebergs should not fall below 100 m or 200 m. This is supported by recently published observations that icebergs less than 100 m long account for only 1% of the reported iceberg volume (Jacka and Giles, 2007). Second, the frequency distribution of Gladstone et al. (2001) is derived from ship observations and therefore represents icebergs in a state of decay rather than their original size at the calving site. Applying a continuous iceberg size distribution in conjunction with a random number simulator to the calving problem would be an obvious alternative.

A step further would be to include giant icebergs in the simulation, i.e. icebergs exceeding 8 km in length. Silva et al. (2006) showed the importance of these large icebergs, which account for half of the fresh-water flux released from icebergs and melt farther away from the shelf area surviving much longer in or across the Antarctic Circumpolar Current. However, such giant icebergs do not calve regularly but result from great ice-shelf break-up events and are thus not easy to parameterize. There is no immediately obvious solution to implement giant icebergs in a CGCM because on the one hand a prescribed calving such as in Silva et al. (2006) reduces the freedom of the CGCM and on the other hand the calving process as it is presently understood is too complex for a CGCM suitable parameterization even with a coupled ice-sheet model available.

All of the snow discharge is currently used to form icebergs. However, parts of it could or should enter the ocean via ice-shelf bottom melt. In order to realize this, some representation of ice-shelf cavities needs to be introduced to the CGCM. Although iceberg calving and ice-shelf bottom melt have been identified as the major pathways for mass loss of the great ice sheets (Lemke et al., 2007) the ratio between these two is still under discussion as measurements or estimates of ice-shelf bottom melt are rare but their number and quality is increasing.

For this study the maximum thickness of icebergs at the moment of calving is set to 250 m following Gladstone et al. (2001). However, the initial thickness should be a function of the average thickness of the ice shelf or glacier that the iceberg originates from and also depend on the local bathymetry used in the CGCM.

To this point we consider grounding of icebergs only partially. Icebergs may run aground in two different ways. Horizontally, they may interact with the coast, and vertically they can ground in shallow areas of the continental shelf (Bigg et al., 1997). The former is included in our model and allows the icebergs to creep along the coast, i.e. we consider only the displacement of the Lagrangian particle that is parallel to the coast whenever an iceberg hits land. Including the latter requires a reasonable bathymetry. Allowing larger icebergs that approach the continental shelf from deeper waters and that greatly exceed the water depth on the shelf to creep along the shelf edge like along a coastline could strengthen the impact of the icebergs because it would prevent them from melting on the continental shelf. This could, in particular, impact the Weddell Sea where icebergs enter from the east and leave to the north with the gyre current.

We also did not consider interactions between icebergs themselves. Collisions may become a major force, in particular in coastal regimes (MacAyeal et al., 2008). In the presence of sea-ice concentrations exceeding 85% or 95% icebergs may get locked into the dense sea-ice cover (Lichey and Hellmer, 2001; Schodlok et al., 2006). However, sea ice may not always act as a collector of the wind momentum (Aoki, 2003). The locking of icebergs has been simulated by Lichey and Hellmer (2001) with an uncoupled

large-scale sea-ice model in a discontinuous manner. A possibility to force the coherent motion of icebergs and sea ice would be to use a variable sea-ice drag coefficient in the momentum balance of the icebergs, which grows exponentially with sea-ice concentration.

Although the individual weight of the icebergs imposes a pressure on the ocean in our model the Lagrangian particles do not cover any area but are simply points in space on the Eulerian grid of the CGCM. Considering an areal extent of the icebergs would be most important for the global albedo because icebergs often have a brighter surface than their surroundings, in particular in open water.

A major simplification in our model is that icebergs interact only with the surface layer of the ocean. As icebergs may penetrate the ocean to depths of several hundred meters the iceberg model would need the full 3-D fields of ocean temperature and current speeds to better reflect reality. The exchanged fresh-water field would need to become a 3-D array, too, because the melt water is naturally not only entrained in the surface layer as is the case in the current model. Both, the dynamic interaction of a full 3-D iceberg body and the release of fresh water at depth would then affect the ocean's stratification. The associated small-scale turbulence in the surroundings of the iceberg might enhance mixing over greater depths but will need to be parameterized. However, the overall impact of this simplification is limited because the dominant melt term in the mass balance of the icebergs, wave erosion, is a surface process.

Finally, the model lacks the true time scale of an ice sheet though our approach includes a buffer, which de-couples the seasonal cycles of snow fall over the continent and fresh-water discharge to the ocean (Fig. 1). Hence, for climate change scenarios a change in iceberg calving indicates rather a change in precipitation over ice covered land masses than a change of ice-sheet or ice-shelf behaviour. Nevertheless, a generally warmer ocean in a climate change scenario strongly impacts the iceberg melt behaviour and the iceberg mass accumulated on the ocean.

## 5. Conclusions

We have shown that the parameterization of the frozen fresh-water flux from land to ocean with simplified Lagrangian icebergs can successfully be applied in a fully coupled model environment. The new parameterization is a more realistic closure of the fresh-water cycle at the land-ice ocean interface because it considers the dynamic and thermodynamic processes—transport and slow melt—related to the discharge of frozen water. Icebergs are, besides ice-shelf bottom melt, the major pathway for ice-sheet mass loss. In contrast to any prescribed fresh-water distribution the fully coupled icebergs allow the model to freely develop the balance between precipitation, calving, and melt water flux as well as the forcing of melt processes, such as ocean temperature and wind speeds.

We found that the implementation of icebergs into a CGCM importantly affects the timing and spatial distribution of the melt water flux. The snow discharge is greatest during the winter season whereas iceberg melt peaks in summer. Furthermore, the spatial distributions of iceberg mass and melt water have a strong gradient perpendicular to the coast with decreasing magnitude towards the open sea. Both aspects, time and location, importantly affect the sea-ice cover and dense water formation. The sea-ice cover is thinner and less compact with icebergs compared to the control experiment. In the latter the snow discharge enters the ocean at the coast, stimulating sea-ice growth. In contrast, Jongma et al. (2009) report a sea-ice growth enhancing effect of the iceberg melt water because in their control experiments the authors either ne-



glect snow discharge or redistribute the associated fresh-water homogeneously over the Southern Ocean area. Hence, we conclude that the handling of the snow discharge in coupled models is important for biases without icebergs.

In our experiments the reduced fresh-water input over continental-shelf regions in experiments with icebergs and in particular with bergy bits enhances the deep and bottom water formation. This change is strongest in the Weddell and Ross seas. We find a 10% increase (1 Sv) of AABW production, which agrees well with Jongma et al. (2009). We found that similarly dense waters may form in the control experiment but these are due to open water convection in contrast to the enhanced shelf convection in the iceberg experiments. The distinction between these formation processes has significant implications for biogeochemical processes, particularly for carbon uptake.

In general, the impact of introducing icebergs are much greater on the southern than on the northern hemisphere, because about 90% of the global iceberg mass originates from Antarctica. In the northern hemisphere most icebergs originate from Greenland, where glaciers calve into the Greenland and Labrador seas. Hence, the Arctic Ocean and its sea-ice cover are not significantly affected. The deep-water formation in the North Atlantic depends more on cooling of the surface ocean by winds than on salinization by sea-ice formation and therefore the icebergs have a much weaker impact than in the Weddell or Ross seas.

Despite known shortcomings the iceberg parameterization as described here will be used at GFDL in model scenarios for the next IPCC Assessment Report. The development of an ice-sheet model to be coupled to the CGCM will offer new opportunities to better simulate iceberg and ice-shelf bottom melt processes. The introduction of freely evolving icebergs in a CGCM also opens up possibilities in palaeoclimate simulations (e.g. Wiersma and Jongma, 2009) or biogeochemical model studies. For instance, it has been shown that icebergs play a role in the ecosystem of the (sub-) polar oceans (e.g. Raiswell et al., 2008; Lancelot et al., 2009). The release of sediments, namely iron during iceberg melt stimulates phytoplankton growth.

## Acknowledgements

We thank Stephen Griffies, Bob Hallberg and Mike Winton for valuable discussions. This study was inspired by results obtained by Eric Galbraith who was experimenting with distributing the calving over the open ocean away from the coasts in a low resolution coupled model. We also like to thank NOAA/GFDL for providing the computational infrastructure to run the CGCM experiments. This report was prepared by Torge Martin under award NA17RJ2612 and NA08OAR4320752 from the National Oceanic and Atmospheric Administration, US Department of Commerce. The statements, findings, conclusions, and recommendations are those of the authors and do not necessarily reflect the views of the National Oceanic and Atmospheric Administration, or the US Department of Commerce.

## Appendix A. Iceberg model equations

The motion of fluids in a CGCM are generally described from an Eulerian point of view. In contrast, we treat icebergs as Lagrangian objects, which are considered points in space. The present model mainly resembles that of Bigg et al. (1997) and Gladstone et al. (2001) though deviating in some aspects. Physically reasonable modifications proved to enhance numerical stability of the model. Most notably, we revised the formula of the wave radiation force.

Icebergs are approximated as cuboids with total thickness  $T$ , length  $L$  and width  $W$ . This simplifies the calculation of the differ-

ent working surfaces in the momentum and mass balance equations. The total thickness is divided into freeboard  $F$ , which is height above water level, and draught  $D$ , the submerged depth of the iceberg, with  $T = F + D$  and  $D = \rho/\rho_o T \simeq 0.8T$ . Here, we assume an average density of  $\rho = 850 \text{ kg m}^{-3}$  for all icebergs (Silva et al., 2006) and an average density of seawater  $\rho_o = 1025 \text{ kg m}^{-3}$ .

The momentum balance for an iceberg of mass  $M$  is given by

$$M \frac{d\vec{v}}{dt} = -M\vec{f} \times \vec{v} + \vec{\tau}_a + \vec{\tau}_o + \vec{\tau}_i + \vec{F}_r + \vec{F}_p \quad (\text{A.1})$$

where  $d/dt = \partial/\partial t + \vec{\nabla} \cdot \vec{v}$  is the absolute derivative in time and  $\vec{f}$  denotes the Coriolis parameter. The momentum balance comprises drag forces for atmosphere, ocean and sea ice:

$$\vec{\tau}_a = \rho_a (0.5c_{a,v}WF + c_{a,h}LW) |\vec{v}_a - \vec{v}|(\vec{v}_a - \vec{v}) \quad (\text{A.2a})$$

$$\vec{\tau}_o = \rho_o (0.5c_{o,v}W(D - T_i) + c_{o,h}LW) |\vec{v}_o - \vec{v}|(\vec{v}_o - \vec{v}) \quad (\text{A.2b})$$

$$\vec{\tau}_i = \rho_i 0.5c_{i,v}WT_i |\vec{v}_i - \vec{v}|(\vec{v}_i - \vec{v}) \quad (\text{A.2c})$$

where indexes  $a$ ,  $o$  and  $i$  refer to atmosphere, ocean and sea ice, respectively,  $\rho_x$  with  $x = \{a, o, i\}$  denotes density, and  $c_{x,v}$  and  $c_{x,h}$  are the associated vertical and horizontal drag coefficients. Following Gladstone et al. (2001) we set  $c_{a,v} = 1.3$ ,  $c_{a,h} = 0.0055$ ,  $c_{o,v} = 0.9$ , and  $c_{o,h} = 0.0012$ . Sea ice acts only on the side walls of the iceberg, playing a minor role because its thickness  $T_i$  is much smaller than  $D$  for most of the iceberg's life-time. The drag coefficient  $c_{i,v}$  is assumed to equal  $c_{o,v}$ . The respective working surfaces were not explicitly mentioned by Bigg et al. (1997) and Gladstone et al. (2001) and thus may be different here.

The iceberg is further driven by the wave radiation force

$$\vec{F}_r = \frac{1}{2} \rho_o c_r g a \min(a, F) \frac{2LW}{L+W} \frac{\vec{v}_a}{|\vec{v}_a|} \quad (\text{A.3})$$

where  $g$  is the acceleration due to gravity and  $a$  denotes the wave amplitude, which is empirically related to the wind speed. Here, we considerably deviate from the studies of Bigg et al. (1997) and Gladstone et al. (2001) as we

- (1) consider only the wind speed relative to the ocean current in the equation for the wave amplitude  $a = 0.010125|\vec{v}_a - \vec{v}_o|^2$ , while we still assume that surface waves travel in the same direction as the wind,
- (2) consider that the wave radiation force decreases when the freeboard of the iceberg  $F$  becomes smaller than the waves ( $F < a$ ),
- (3) account for a varying ratio of the length  $L$  and width  $W$  of the icebergs by using the harmonic mean of  $L$  and  $W$ , which varies between  $W$  and  $2W$ , in the determination of the working surface, and
- (4) apply a variable coefficient  $c_r$  that damps the wave radiation force when the ratio of iceberg length and wavelength becomes small. We defined the wave radiation coefficient  $c_r$  as

$$c_r = 0.06 \min \left( \max \left[ 0, \frac{L - L_c}{L - L_c} \right], 1 \right) \quad (\text{A.4})$$

where the cutoff length  $L_c = 0.125L_w$  and the upper limit  $L_t = 0.25L_w$  are chosen to resemble the curve presented by Carrieres et al. (2001, their Fig. 6) with the wavelength empirically derived from  $L_w = 0.32|\vec{v}_a - \vec{v}_o|^2$ .

We found the above changes to be important in stabilizing the model as the wave radiation force can become the dominant driving force.

Finally a pressure gradient force is considered

$$\vec{F}_p = -Mg\vec{\nabla}\eta \quad (\text{A.5})$$

that includes the effect of the sea surface slope  $\eta$  to the momentum balance of the icebergs.



The mass balance of an iceberg is given by

$$\rho \frac{d(LWT)}{dt} = \rho(-LWM_b - T(L+W)(M_e + M_v)) \quad (\text{A.6})$$

Gladstone et al. (2001) stated that the melt and erosion of an iceberg are mainly driven by bottom melt  $M_b$ , wave erosion  $M_e$  and buoyant convection at the side walls  $M_v$  and that all other effects are negligible small. Therefore, we focused on these three effects. Again, the above equation may be different from the approaches of Bigg et al. (1997) and Gladstone et al. (2001) with respect to the working surfaces applied. All melt terms have units of meters per day.

At the base of an iceberg, turbulence is created by the relative motion of the water passing the iceberg. Since the effective iceberg temperature  $\tilde{T}$  is assumed to be constantly at  $-4^\circ\text{C}$  (Løset, 1993) this turbulence generates a heat flux to the iceberg. The associated melt rate is estimated by

$$M_b = 0.58 |\vec{v} - \vec{v}_o|^{0.8} \frac{\tilde{T}_o - \tilde{T}}{L^{0.2}} \quad (\text{A.7})$$

where  $\tilde{T}_o$  is the sea surface temperature.

The reduction in iceberg volume due to wave erosion is assumed to be directly proportional to the sea state  $S_s$  and the sea surface temperature  $\tilde{T}_o$ , which always has a positive impact because  $\tilde{T}_o > \tilde{T}$ ,

$$M_e = \frac{1}{12} S_s (1 + \cos[\pi A_i^3]) (\tilde{T}_o + 2) \quad (\text{A.8})$$

However, wave erosion decreases with increasing sea-ice coverage because an ice cover damps waves and reduces the wind fetch. Therefore, Gladstone et al. (2001) included a dependence on the fractional sea-ice area  $A_i$ . The above empirical function of wave erosion includes calving of slabs from the iceberg (Bigg et al., 1997). We estimate the sea state by a fit to the Beaufort scale:

$$S_s = \frac{3}{2} |\vec{v}_a - \vec{v}_o|^{1/2} + \frac{1}{10} |\vec{v}_a - \vec{v}_o| \quad (\text{A.9})$$

The permanent temperature contrast between the iceberg and the ocean results in buoyant convection along the side walls of the iceberg. The related heat transfer is a non-negligible contributor to the reduction of iceberg mass. The melt rate of this process was empirically estimated to be

$$M_v = 7.62 \times 10^{-3} \tilde{T}_o + 1.29 \times 10^{-3} \tilde{T}_o^2 \quad (\text{A.10})$$

by El-Tahan et al. (2001).

Like Bigg et al. (1997) we apply the empirical criterion of Weeks and Mellor (1978)

$$L < \sqrt{0.92D^2 + 58.32D} \quad (\text{A.11})$$

to allow icebergs to roll over. In this case  $W$  and  $T$  are instantaneously swapped.

## References

- Anderson, J.L. et al., 2004. The new GFDL global atmosphere and land model AM2-LM2: evaluation with prescribed SST simulations. *J. Climate* 17, 4641–4673.
- Aoki, S., 2003. Seasonal and spatial variations of iceberg drift off Dronning Maud Land, Antarctica, detected by satellite scatterometers. *J. Oceanogr.* 59, 629–635.
- Bigg, G.R., Wadley, M.R., Stevens, D.P., Johnson, J.A., 1997. Modelling dynamics and thermodynamics of icebergs. *Cold Reg. Sci. Technol.* 26, 113–135.
- Boville, B.A., Gent, P.R., 1998. The NCAR climate system model, version one. *J. Climate* 11, 1115–1130.
- Carrieres, T., Sayed, M., Savage, S., Crocker, G., 2001. Preliminary verification of an operational iceberg drift model. In: POAC '01. Proc. 16th Intl. Conf. Port and Ocean Engineering under Arctic Conditions, pp. 1107–1116.
- Cavaliere, D.J., Parkinson, C.L., 2008. Antarctic sea ice variability and trends, 1979–2006. *J. Geophys. Res.*, 113.
- Delworth, T.I. et al., 2006. GFDL's CM2 global coupled climate model. Part I: Formulation and simulation characteristics. *J. Climate* 19, 643–674.
- El-Tahan, M.S., Venkatesh, S., El-Tahan, H., 2001. Validation and quantitative assessment of the deterioration mechanisms of Arctic icebergs. *J. Offshore Mech. Arct. Eng.* 109, 102–108.
- Gerdes, R., Hurlin, W., Griffies, S.M., 2006. Sensitivity of a global ocean model to increased run-off from Greenland. *Ocean Modell.* 12, 416–435.
- Gladstone, R.M., Bigg, G.R., Nicholls, K.W., 2001. Iceberg trajectory modeling and meltwater injection in the Southern Ocean. *J. Geophys. Res.* 106 (C9), 19903–19915.
- Goose, H., Fichfet, T., 1999. Importance of ice–ocean interactions for the global ocean circulation: a model study. *J. Geophys. Res.* 104 (C10), 23337–23355.
- Gordon, C., Cooper, C., Senior, C.A., Banks, H., Gregory, J.M., Johns, T.C., Mitchell, J.F.B., Wood, R.A., 2000. The simulation of SST, sea ice extents and ocean heat transports in a version of the Hadley Centre coupled model without flux adjustments. *Clim. Dyn.* 16, 147–168.
- Hack, J.J., Caron, J.M., Yeager, S.G., Oleson, K.W., Holland, M.M., Truesdale, J.E., Rasch, P.J., 2006. Simulation of the global hydrological cycle in the CCSM Community Atmosphere Model Version 3 (CAM3): mean features. *J. Climate* 19, 2199–2221.
- Hallberg, R., 1995. Some Aspects of the Circulation in Ocean Basins with Isopycnals Intersecting the Sloping Boundaries. Ph.D. Thesis. University of Washington.
- Hallberg, R., Gnanadesikan, A., 2006. The role of eddies in determining the structure and response of the wind-driven southern hemisphere overturning: results from the Modeling Eddies in the Southern Ocean (MESO) project. *J. Phys. Oceanogr.* 36, 2232–2252.
- Hibler III, W.D., 1979. A dynamic–thermodynamic sea ice model. *J. Phys. Oceanogr.* 9 (4), 815–846.
- Hooke, R.L., 2005. Principles of Glacier Mechanics, second ed. Cambridge University Press.
- Hunke, E.C., Dukowicz, J.K., 1997. An elastic–viscous–plastic model for sea ice dynamics. *J. Phys. Oceanogr.* 27, 1849–1867.
- Jacka, T.H., Giles, A.B., 2007. Antarctic iceberg distribution and dissolution from ship-based observations. *J. Glaciol.* 53 (182), 341–356.
- Jacobs, S.S., Helmer, H.H., Doake, C.S.M., Jenkins, A., Frolich, R.M., 1992. Melting of ice shelves and the mass balance of Antarctica. *J. Glaciol.* 38 (130), 375–387.
- Jongma, J.I., Driesschaert, E., Fichfet, T., Goose, H., Renssen, H., 2009. The effect of dynamic–thermodynamic icebergs on the southern ocean climate in a three-dimensional model. *Ocean Modell.* 26 (1–2), 104–113.
- Lancelot, C., de Montety, A., Goose, H., Becquevort, S., Schoemann, V., Pasquer, B., Vancoppenolle, M., 2009. Spatial distribution of the iron supply to phytoplankton in the Southern Ocean: a model study. *Biogeosciences* 6, 2861–2878.
- Lemke, P., Ren, J., Alley, R., Allison, I., Carrasco, J., Flato, G., Fujii, Y., Kaser, G., Mote, P., Thomas, R., Zhang, T., 2007. Observations: changes in snow, ice and frozen ground. In: Solomon, S., Qin, D., Manning, M., Chen, Z., Marquis, M., Averyt, K., Tignor, M., Miller, H. (Eds.), *Climate Change 2007: The Physical Science Basis. Contribution of Working Group I to the Fourth Assessment Report of the Intergovernmental Panel on Climate Change*. Cambridge University Press, Cambridge, United Kingdom and New York, NY, USA, pp. 337–383.
- Lichey, C., Hellmer, H.H., 2001. Modeling giant iceberg drift under the influence of sea ice in the Weddell Sea. *J. Glaciol.* 47, 452–460.
- Løset, S., 1993. Thermal energy conservation in icebergs and tracking by temperature. *J. Geophys. Res.* 98 (C6), 10001–10012.
- MacAyeal, D.R., Okal, M.H., Thom, J.E., Brunt, K.M., Kim, Y.-J., Bliss, A.K., 2008. Tabular iceberg collisions within the coastal regime. *J. Glaciol.* 54 (185), 371–386.
- Meehl, G., Stocker, T., Collins, W., Friedlingstein, P., Gaye, A., Gregory, J., Kitoh, A., Knutti, R., Murphy, J., Noda, A., Raper, S., Watterson, I., Weaver, A., Zhao, Z.-C., 2007. Global climate projections. In: Solomon, S., Qin, D., Manning, M., Chen, Z., Marquis, M., Averyt, K., Tignor, M., Miller, H. (Eds.), *Climate Change 2007: The Physical Science Basis. Contribution of Working Group I to the Fourth Assessment Report of the Intergovernmental Panel on Climate Change*. Cambridge University Press, Cambridge, United Kingdom and New York, NY, USA, pp. 747–845.
- Oleson, K.W. et al., May 2004. Technical Description of the Community Land Model (CLM). Tech. Rep. NCAR/TN-461+STR. National Center for Atmospheric Research, Boulder, CO, 174 pp.
- Opsteegh, J.D., Haarsma, R.J., Selten, F.M., Kattenberg, A., 1998. ECBILT: a dynamic alternative to mixed boundary conditions in ocean models. *Tellus Series A* 50 (3), 348–367.
- Raiswell, R., Benning, L.G., Tranter, M., Tulaczyk, S., 2008. Bioavailable iron in the Southern Ocean: the significance of the iceberg conveyor belt. *Geochim. Trans.* 9 (7).
- Reynolds, R.W., Rayner, N.A., Smith, T.M., Stokes, D.C., Wang, W., 2002. An improved in situ and satellite SST analysis for climate. *J. Climate* 15, 1609–1625.
- Rignot, E., Jacobs, S.S., 2002. Rapid bottom melting widespread near Antarctic ice sheet grounding lines. *Science*, 296.
- Rignot, E., Kanagaratnam, P., 2006. Changes in the velocity structure of the Greenland ice sheet. *Science* 311, 986–990.
- Schodlok, M.P., Hellmer, H.H., Rohardt, G., Fahrback, E., 2006. Weddell Sea iceberg drift: five years of observations. *J. Geophys. Res.*, 111.
- Silva, T.A.M., Bigg, G.R., Nicholls, K.W., 2006. Contribution of giant icebergs to the Southern Ocean freshwater flux. *J. Geophys. Res.*, 111.
- Stammer, D., 2008. Response of the global ocean to Greenland and Antarctic ice melting. *J. Geophys. Res.*, 113.
- Tsunogai, S., Watanabe, S., Sato, T.E., 1999. Is there a “continental shelf pump” for the absorption of atmospheric CO<sub>2</sub>? *Tellus Series B* 51 (3), 701–712.
- Weber, S.L., Drijfhout, S.S., Abe-Ouchi, A., Crucifix, M., Eby, M., Ganopolski, A., Murakami, S., Otto-Bliesner, B., Peltier, W.R., 2007. The modern and glacial

- overturning circulation in the Atlantic Ocean in PMIP coupled model simulations. *Clim. Past*, 3, 51–64.
- Weeks, W.F., Mellor, M., 1978. Some elements of iceberg technology. In: Hussein, A.A. (Ed.), *Proceedings of the First Conference on Iceberg Utilization for Freshwater Production*, Iowa State University, pp. 45–98.
- Wiersma, A.P., Jongma, J.L., 2009. A role for icebergs in the 8.2 ka climate event. *Clim. Dyn.*
- Winton, M., 2000. A reformulated three-layer sea ice model. *J. Atmos. Ocean. Technol.* 17, 525–531.
- WMO, 1989. *WMO Sea-Ice Nomenclature*, fifth ed. World Meteorological Organization, Secretariat of the WMO, Geneva, Switzerland.
- Worby, A.P., Geiger, C.A., Paget, M.J., Woert, M.L.V., Ackley, S.F., DeLiberty, T.L., 2008. Thickness distribution of Antarctic sea ice. *J. Geophys. Res.*, 113.